Bonding structure and mechanical properties of Ti-B-C coatings

Manuel David Abad[1], Daniel Cáceres[2], Yury S. Pogozhev[3],
Dmitry V. Shtansky[3], Juan Carlos Sánchez-López[1,*]

[1]*Instituto de Ciencia de Materiales de Sevilla (CSIC-Universidad de Sevilla), Avda. Américo Vespucio 49, 41092-Sevilla, Spain*
[2]*Departamento de Física, Universidad Carlos III (Madrid), Avda. de la Universidad 30, 28911-Leganés (Madrid), Spain*
[3]*State Tecnological University "Moscow Institute of Steel and Alloys", Leninsky pr. 4, 119049-Moscow, Russia*

Abstract

Nanocomposite coatings combining hard phases (TiB_2, TiC) with amorphous carbon (a-C) were developed to provide a good compromise between mechanical and tribological properties for M2 steels used in a wide variety of applications such as cutting tools, bearings and gear mechanisms. A combined d.c.-pulsed and r.f.-magnetron deposition process was used to deposit nanocomposite TiBC/a-C coatings with a variable content of carbon matrix phase. Chemical composition was determined by electron energy-loss spectroscopy (EELS) and X-ray photoelectron spectroscopy (XPS). Transmission electron microscopy (TEM) revealed that the coatings microstructure is rather amorphous with small nanocrystals of TiC and/or TiB_2 (not possible to differentiate by diffraction techniques). Investigation of the chemical bonding environment by XPS and EELS allows us to confirm the presence of titanium-boron and titanium-carbon bonds together with free amorphous carbon. Coatings exhibited hardness values (H) of 25–29 GPa, effective Young modulus (E*) of 310-350 GPa, H/E* ratios over 0.080 and resistance to plastic deformation (H^3/E^{*2}) from 0.15 to 0.20. Tribological properties of the coatings were characterized by a pin-on-disk tribometer using steel and WC balls at high contact stresses (1.1 and 1.4 GPa respectively). Friction coefficients were reduced from 0.6 to 0.2 by increasing the content of free carbon without reduction of the hardness (around 28 GPa), by self-lubricant effects. The tribomechanical data are revised according to the phase composition and chemical bonding inside the nanocomposites.

Keywords: magnetron sputtering, TiBC coatings, EELS, XPS, mechanical properties.

*E-mail corresponding author: jcslopez@icmse.csic.es

† Dedicated to D. Cáceres who suddenly passed away during the preparation of this work

Introduction

Nanocomposite coatings materials have recently attracted increasing interest due to the possibility of the synthesis of materials with unique properties, e.g. super-hardness[1-3] , combined hardness and low friction[4,5], or "chamaleonic" or surface adaptative.[6,7] TiB_2, Ti-B-X (with X: C, N) and transition-metal-based composite coatings are attractive due to their high hardness, high melting point and their unique functional properties as high wear and corrosion resistance.[8-10] Many other research groups have investigated ternary Ti-B-C coatings using various deposition methods.[11-23] Ti-B-C coatings have been deposited by chemical vapour deposition (CVD)[11,12] and physical vapour deposition (PVD) by many different processes.[13-23] Reactive magnetron sputtering (MS) from a target of TiB_2 with different carbon gaseous precursors has been investigated.[13,14] Ti-B-C system has also been obtained by non-reactive sputtering by using two targets (TiB_2 and C)[15-17] or a unique combined target (Ti-B-C).[20-23] The coefficient of friction of such TiB_2–based coatings is usually high, namely 0.6, especially when compared to diamond-like-carbon (DLC)[24] and other carbon containing coatings for which coefficients of friction are approximately 0.1.[25] In an attempt to improve the friction and wear properties of TiB_2–based coatings, composite coatings, multilayered, and multiphase coatings have been investigated.[5,11-13,16-20] Gilmore et al. reported on multilayered TiB_2 and co-sputtered TiB_2-C coatings (namely Ti-B-C coatings) and found that an overall carbon concentration as high as 50 at. % is required to reduce the coefficient of friction.[17]

In this current work, novel Ti-B-C coatings were synthesized by non-reactive magnetron sputtering from two targets: one of a determined composition of TiC:TiB_2 (60:40)

and another of graphite, with the aim of improving the tribological properties by tuning the free carbon matrix inside the Ti-B-C coating. An exhaustive chemical investigation is carried out with the aim of identifying the types of bonding inside the coatings and their correlation with the friction properties.

Experimental Part

Ceramic targets of $TiC:TiB_2$ (hereafter namely TiBC) were produced in a ratio 60:40 using the self-propagating high-temperature synthesis method (SHS) described in more detail in reference [21]. The elemental composition was found in 42.4 at. % of Ti, 30.8 at. % of B and 26.8 at. % of C and the residual porosity around 7.5%. The Ti-B-C coatings were prepared by Ar^+ sputtering of the combined TiBC and graphite targets. The magnetron sources were r.f. (graphite target, Goodfellow, 99.5%) and pulsed d.c. (TiBC target) at frequencies of 13.56 MHz and 50 kHz respectively. The pressure of the vacuum chamber was measured before deposition in 3×10^{-4} Pa and 0.60 Pa while growing. A series of Ti-B-C coatings has been prepared by changing the sputtering power ratio (R), defined as the ratio of sputtering power applied to the graphite target in respect to the TiBC one ($R= P_C/P_{TiBC}$), from 0 to 2. The typical power values applied to the TiBC target span between 125 and 250 W while those applied to the graphite target were varied from 0 to 250 W. All the films begin with a first step (underlayer) by single sputtering of the TiBC target at 250 W. Second, the magnetron with the graphite target is switched on and the selected values of sputtering power for each target are fixed for deposition of the Ti-B-C coatings as summarized in Table 1. The substrates were mounted in a rotary sample-holder situated at 10 cm from the target. A rotation speed of 10 rpm is used to ensure homogeneity. The temperature was found to vary in the range of 150–200 °C under the effect of the plasma. No additional heating of the substrate was done. A negative bias of 100V was applied to the samples during whole deposition process. The growth time was around 5 hours and the film thickness ranges from 1.5 to 2.0

μm. The substrates used were silicon, M2 steel and NaCl for TEM images depending on the characterization technique.

The crystal structure of the films was examined by X-ray diffraction analysis (XRD) at a low incidence angle of 1° in order to increase the signal from the coating compared with the substrate. X-Ray diffraction measurements were carried out using Cu K_α radiation in a Siemens D5000 diffractometer. Scanning electron microscopy (SEM) observations were done with a SEM FEG Hitachi S4800 equipment. Transmission electron microscopy (TEM), electron diffraction (ED) and electron energy loss spectroscopy (EELS) analyses were carried out in a Philips CM200 microscope operating at 200 kV and equipped with a parallel detection EELS spectrometer from Gatan (766-2 K). For their observation, the films were grown on NaCl substrates and then floated off in water and supported on a copper grid. The B, C, O and Ti core-loss edges were recorded in the diffraction mode with a camera length of 470 mm. Using a 2-mm spectrometer, entrance aperture yielded an energy resolution at the zero-loss peak of 1.4 eV. Spectra were recorded for dark current and channel-to-channel gain variation. Commercial TiC powder and an amorphous carbon were measured in the same conditions to be used as reference compounds. After subtraction of the background by a standard power-law function, the spectra were deconvoluted for plural scattering with the Fourier-ratio method and normalized to the jump. All of these treatments were performed within the EL/P program (Gatan). X-ray photoelectron spectroscopy (XPS) measurements were carried out using a Leybold-Heraeus spectrometer equipped with an EA-200 hemispherical electron multichannel analyzer operating with a non-monochromated Mg K_α X-ray source (1253.6 eV). An Ar^+ sputtering at 3 kV and a pressure of 2×10^{-6} Pa during 5 min was previously carried out in order to remove the surface contamination. These conditions were found as most appropriate to remove preferentially the hydrocarbon surface contamination layer without affecting the film elemental composition. The C1s line of 284.5 eV binding energy was used as a reference to correct the binding energies for the charge shift.

Tribological tests were carried out using 6 mm-diameter 100Cr6 steel and WC balls in a pin-on-disk CSM tribometer with a sliding speed of 10 cm/s and 5 N of applied load in ambient air (30–60% of relative humidity). The sliding distance was 1000 m with typical track radius between 6 and 10 mm. Nanoindentation experiments were performed with a Nanoindenter II (Nano Instruments, Inc., Knoxville, TN) mechanical properties microprobe. All tests were performed at room temperature with a diamond Berkovich (three-sided pyramid) indenter tip. Each specimen was tested using the continuous stiffness measurement technique developed by Pethica and Oliver.[26,27] The maximum load was selected in such a way that the maximum indentation depth did not exceed 10–15% of the coating thickness in order to avoid the influence of the substrate.

Results and Discussion

Chemical composition

The Ti-B-C coating chemical compositions obtained by EELS are summarized in Table 1. It can be seen how the increasing the sputtering power of the graphite target the carbon concentration was varied between 31 and 61 at. %. The oxygen impurities were found to be a little high for low ratios (R0 R0.2, R0.5) around 12%. Similar values of oxygen were found in references. [12, 28] When the incorporation of carbon was more significant (ratios above 1), the average oxygen impurity is observed to be about 2-4%. It is believed that the oxygen impurity comes from the SHS target and additional absorption by titanium atoms.

Figure 1 collects the elemental composition of the prepared coatings and the initial TiBC target on a ternary diagram. It is observed a slight difference between the target composition and the coating R0, obtained by direct sputtering of this target, which could be explained by different energies of the sputtered and different thermalization and scattering behaviour. For the low ratios (0 and 0.5), the chemical composition represents just a small deviation from the quasibinary tie line TiB_2-TiC, meanwhile, at higher ratios the composition of the coating

appears inside the TiB_2-TiC-C region where the three phases can coexist as a consequence of the carbon incorporation.

Microstructure and chemical bonding

Figure 2(a) shows a SEM cross-section observation of R2 sample as representative for all the series of coatings deposited within this work. Two layers are clearly observed corresponding to the underlayer (similar synthesis conditions to R0) and coating itself respectively. A change of morphology is noticed towards a more dense featureless structure. This result was further confirmed by TEM planar view observation of the same sample. Figure 2(b) reveals a finer grain structure in the R2 coating than R0 whereas some fine agglomerates of 10-15 nm are observed. These morphologies can not be correlated with crystalline features as can be inferred from the ED analysis taken for these areas. Indeed, the electron diffraction pattern from R0, exhibits a diffuse halo indicating an amorphous nature of this layer whilst the coating R2, with the double of carbon content, some rings are now observed. This supposes an increment of the coatings crystallinity along with the increase of the carbon content. This could be explained by the formation of some crystalline phases of TiB_2 or TiC but their d-spacings are very close and it is not possible to distinguish them accurately. Moreover, some authors have postulated the formation of a metastable monophase Ti-B-C compound when two- or multiphase target materials such as TiC+TiB_2 are used. [23]

The results of GIXRD analysis on the coatings is represented in the Figure 3. The diffractograms shown for Ti-B-C coating did not reveal well-defined diffraction patterns except the peak at 44° (2θ) originated by the steel substrate and very broad band at 35º (2θ) as seen in other works.[11,14,17] By comparing the diffractrograms with the XRD database this peak can be attributed to (100) TiB_2 or (111) TiC planes although the proximity in their main diffraction peaks together with the nanocrystalline or quasi-amorphous character does not

allow to discriminate between them. In addition, as commented before, the broad peak at 35° can be originated from a ternary phase including titanium, carbon and boron. Such a TiB_xC_y phase can be derived either from the hexagonal TiB_2 phase distorted by inclusion of carbon or from the cubic TiC lattice by incorporation of boron.[13,14,22] Similarly to what was observed by electron diffraction technique, it is noticed from the analysis of XRD patterns a gradual increase of the crystallinity at higher C concentration. In agreement with previous results, this can be interpreted by the formation of a ternary TiB_xC_y phase from the introduction of carbon atoms inside the hexagonal TiB_2 lattice.[14]

Investigation of the boron and carbon chemical bonding environment has been carried out by measuring the energy-loss near-edge fine structure (ELNES) of B and C *K*-edges. Figure 4(a) shows the B K-edge spectra for the samples under study revealing the close similarity. The fine structure is dominated by two features: a shoulder around 192 eV (π) and a broad band centred (σ) at 200 eV, in good agreement to what is observed for TiB_2 compounds.[29,30] Figure 4(b) depicts the C K-edge spectra for the same samples together with two references of pure TiC and a-C. The ELNES of TiC is dominated by well separated strong π and σ peaks of approximately equal intensity centred at ~283 eV and 292 eV, respectively. In the case of a-C film the main characteristics are the narrow peak at 285.0 eV and a broad peak centred at 295 eV assigned to the π and σ transitions, respectively. According to the shape and position of the C *K*-edge for the Ti-B-C coatings, the samples can be divided into two groups. In the coatings with less carbon (R0 and R0.5) they seem to be dominated by the carbide features while samples R1 and R2 approach more to the a-C spectrum but maintaining partially the carbide character. In summary, a mixture of TiC and amorphous free carbon should be present with a higher contribution of the latter at increasing ratio. In terms of chemical composition, the variation shown in this figure corresponds to an increment from 31 to 61 at. % of the total carbon content.

In order to obtain complementary information about the chemical state of carbon within the coatings, a deeper insight has been carried out by studying the C1s photoelectron peak. XPS C 1s spectrum of coating R1 (49 at. % of C) is shown in Figure 5 as representative example. The C peak can be composed of three principal components at 282.0, 283.0 and 284.5 eV. The small peak at higher binding energy (286.6 eV) corresponds to C-O bonding. The peak structure was similar for all the coatings varying the relative intensities among the three main peaks. The binding energy for a pure TiC phase is around 282.0 eV and that of amorphous carbon phase is located at 284.5 eV. The predominant peak at 283.0 eV can be due to the incorporation of boron atoms to the TiC phase forming the TiB_xC_y phase whose peak is shifted towards higher energies due to the different Pauling electronegativity between C and B as reported previously by other authors.[16,17,22] Therefore, the XPS analysis allows to conclude that when no more C can be accommodated into the TiB_xC_y phase, this excess appears as a free carbon phase.

Tribo-mechanical properties

The mechanical properties were measured by nanoindentation. As can be observed in Table 1, the coatings exhibited hardness values (H) of 25-29 GPa, effective Young modulus (E*) of 310-350 GPa, H/E* ratio over 0.080 and resistance to plastic deformation (H^3/E^{*2}) from 0.15 to 0.20. There are not significant differences among the mechanical properties depending on the elemental compositions of the coatings although the influence of the carbon in excess for the samples R1 and R2 is manifested in a slight hardness decrease. The formation of a ternary TiB_xC_y phase rather than TiB_2 is detrimental to the mechanical properties of these coatings which show values ranging from 45 to 68 GPa. [9, 30]

Regarding the tribological properties, the measured friction coefficients against either steel or WC balls decrease continuously with the carbon content increment. A minimum total carbon content threshold of about 60 at. % is found for both types of material counterparts to

have friction below 0.3. Below this carbon content, there is not enough free carbon phase to lubricate the contact because it is forming the mixed TiB_xC_y phase. The best compromise between mechanical and tribological properties can be offered by coating R2 (60 at. % C) with hardness (27GPa) and low-friction (0.2-0.3) properties.

Conclusion

A series of Ti-B-C coatings have been deposited by dual magnetron sputtering from graphite and a TiB_2:TiC (40:60) composite target with variable carbon concentrations. X-SEM and TEM images revealed that the coatings microstructure is rather amorphous with small nanocrystals in an amorphous matrix. By X-ray and electron diffraction techniques it is observed a crystalline increase with the carbon content. According to the d-planar spacings, the formation of TiC and/or TiB_2 phases or a ternary TiB_xC_y compound can be foreseen and it is not possible to be distinguished. Investigation of the chemical bonding environment by EELS allows to confirm the contribution of Ti-B and Ti-C mixed in different proportions with amorphous free carbon bonds, higher at increasing sputtering power ratios. XPS measurements of the carbon revealed three main components for the chemical state of the carbon: a-C, TiB_xC_y and TiC. Coatings exhibited high values of hardness (25-29 GPa) and effective Young modulus (310-350 GPa). No big differences in the mechanical properties were found in function of elemental composition although frictions coefficient can be noticeably reduced from 0.6 to 0.2 by increasing the carbon content. This is explained by an increment of the free amorphous carbon, which plays a important role as lubricant, once the formation of the ternary TiB_xC_y is less favoured.

Acknowledgments

The authors are grateful to the Spanish Ministery of Science and Innovation (projects nº MAT2004-01052, MAT2007-66881-C02-01 and CONSOLIDER CSD2008-00023) and European Union (NOE EXCELL NMP3-CT-2005-515703) for financial support.

References

[1] S. Veprek, S. Reiprich, Thin Solid Films **1995**, 268, 64.

[2] S. Veprek, M. Haussmann, S. Reiprich, S. Li, J. Dian, *Surf. Coat. Technol*. **1996**, 86/87, 394.

[3] J. Musil, *Surf Coat* Technol. **2000**, 125, 322.

[4] A. A. Voevodin, J. S. Zabinski, *Diamond Relat.* Mater. **1998**, 7, 463.

[5] S. L. Ma, D.Y. Ma, Y. Guo, B. Xu, G. Z. Wu, K. W. Xu, P. K. Chu, *Acta Mater.* **2007**, 55, 6350.

[6] A. A. Voevodin, J. P. O'Neill, J. S. Zabinsky, *Surf. Coat. Technol*. **1999**, 119, 36.

[7] A. A. Voevodin, T. A. Fitz, J .J. Hu, J. S. Zabinski, *J. Vac. Sci. Technol.* **2002**, 20, 1434.

[8] T. P. Mollart, M. Baker, J. Haupt, A. Steiner, P. Hammer, W. Gissler, *Surf. Coat. Technol*. **1995**, 74/75, 491.

[9] M. Berger. L. Karlsson, M. Larson, S. Hogmark, *Thin Solid Films* **2001**, 401, 179.

[10] R. Wiedemann, V. Weihnacht, H. Oettel, *Surf. Coat. Technol*. **1999**, 116-119, 302.

[11] J.-T. Ok, I.-W. Park, J. J. Moore, M. C. Kang, K. H. Kim, *Surf. Coat. Technol*. **2005**, 200, 1418.

[12] S. Shimada, M. Takahashi, J. Tsujino, I. Yamazaki, K. Tsuda, *Surf. Coat. Technol.* **2007**, 201, 7194

[13] O. Knotek, R. Breidenbach, F. Jungblut, F. Löffler, *Surf. Coat. Technol.* **1990**, 43/44, 107.

[14] C. Mitterer, M. Rauter, P. Rödhammer, *Surf. Coat. Technol.* **1990**, 41**,** 351.

[15] C. Mitterer, P. H. Mayrhofer, M. Beschliesser, P. Losbichler, P. Warbichler, F. Hofer, P. N. Gibson, W. Gissler, H. Hruby, J. Musil, J. Vlček, *Surf. Coat. Technol*. **1999**, 120-121, 405.

[16] M. A. Baker, *Surf. Coat. Technol*. **2007**, 201, 6105.

[17] R. Gilmore, M. A. Baker, P. N. Gibson, W. Gissler, *Surf. Coat. Technol*. **1998**, 105, 45.

[18] J. Rao, R. Cruz, K. J. Lawson, J. R. Nicholls, *Diamond Relat. Mater*. **2005**, 14, 1805.

[19] B. Prakash, E. Richter, H. Pattyn, J. P. Celis, *Surf. Coat. Technol.* **2003**, 173, 150.

[20] D. Zhong, E. Sutter, J. J. Moore, G. G. W. Mustoe, E. A. Levashov, J. Disam, *Thin Solid Films* **2001**, 398-399, 320.

[21] E. A. Levashov, V. I. Kosayanin, L. M. Krukova, J. J. Moore, D. L. Olson, *Surf. Coat. Technol*. **1997**, 92, 34.

[22] I.-W.Park, K. H. Kim, A. O. Kunrath, D. Zhong, J. J. Moore, A. A. Voevodin, E. A. Levashov. *J. Vac. Sci. Technol. B* **2005**, 23, 588.

[23] H. Holleck, M. Lahres, *Mat. Sci. Eng*. **1991**, 140, 609.

[24] A. Erdemir. C. Bindal. C. Zuiker, E. Savrum, *Surf. Coat. Technol*. **1996**, 86-87, 507.

[25] J.C. Sánchez-López, D. Martínez-Martínez, C. López-Cartes, C. Fernández-Ramos, A. Fernández, *Surf. Coat. Technol.* **2005**, 200, 40..

[26] J. B. Pethica, W. C. Oliver, *Mater. Res. Soc. Symp. Proc*. **1989**, 130, 13.

[27] W. C. Oliver, G. M. Pharr, *J. Mater. Res*. **1992**, 7, 1564.

[28] D. Zhong, I-W. Park, A.O. Kunrath, B. Mishra, K.H. Kim, A.A. Voevodin, E.A. Levashov, J.J. Moore, Society of Vacuum Coaters, *48th Annual Technical Conference Proceedings ISSN 0737-5921,* **2005**, 547.

[29] K. Lie, R. Brydson, H. Davock, *Phys. Rev. B* **1999**, 59, 5361.

[30] C. López-Cartes, D. Martínez-Martínez, J. C. Sánchez-López, A. Fernández, A. García-Luis, M. Brizuela, J. I. Oñate**,** *Thin Solid Films* **2007**, 515, 3590.

Table 1. Synthesis conditions, elemental composition measured by EELS and tribo-mechanical properties of the Ti-B-C coatings.

Coating	Synthesis Conditions		Elemental composition				Tribo-mechanical properties					
	P_C	P_{TiBC}	C	B	Ti	Film stoichiometry	H	E*	H/E*	H^3/E^{*2}	μ_{steel}	μ_{WC}
	W	W	%	%	%		GPa	GPa		GPa		
R0	---	250	31	24	45	$TiB_{0.53}C_{0.70}$	24.4	310	0.079	0.151	0.63	0.68
R0.2	50	250	36	17	47	$TiB_{0.36}C_{0.78}$	28.4	350	0.081	0.187	0.61	0.65
R0.5	125	250	40	17	43	$TiB_{0.39}C_{0.90}$	28.3	335	0.084	0.202	0.43	0.61
R1	250	250	49	12	39	$TiB_{0.31}C_{1.27}$	26.3	330	0.080	0.167	0.23	0.40
R2	250	125	61	14	25	$TiB_{0.59}C_{2.48}$	27.0	330	0.082	0.181	0.22	0.28

Figure captions

Figure 1. Elemental composition of the coatings deposited and the initial TiBC target within the system Ti-B-C.

Figure 2. SEM cross-section of R2 sample including underlayer (a); TEM planar views (b) and ED patterns (c) of R0 and R2 coatings.

Figure 3. GIXRD patterns of Ti-B-C coatings with different compositions deposited onto stainless steel substrates.

Figure 4. Boron (a) and carbon (b) *K*-edge EELS spectra of Ti-B-C coatings.

Figure 5. Curve fitted XPS C 1s peak for the Ti-B-C coating R1.

Figure 1

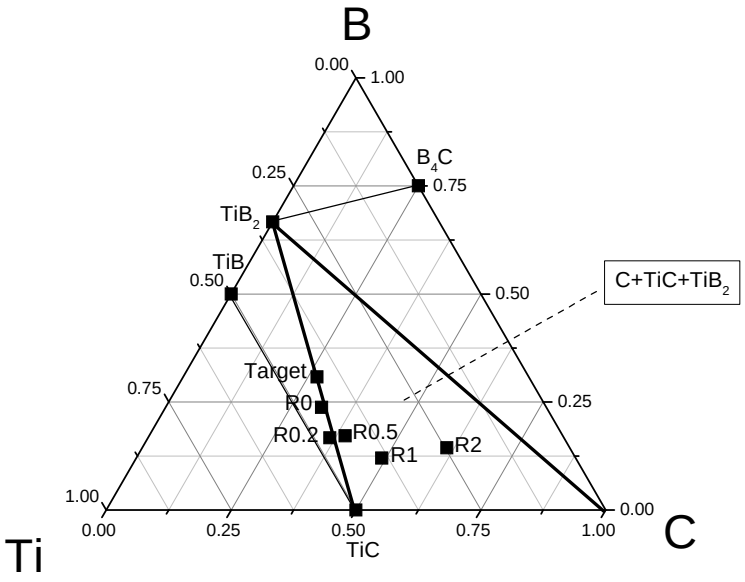
B
0.00
1.00
0.25
0.75
B4C
TiB2
TiB
0.50
0.50
C+TiC+TiB2
Target
0.75
R0
0.25
R0.2
R0.5
R1
R2
1.00
0.00
0.00
0.25
0.50
0.75
1.00
TiC
Ti
C

Figure 2

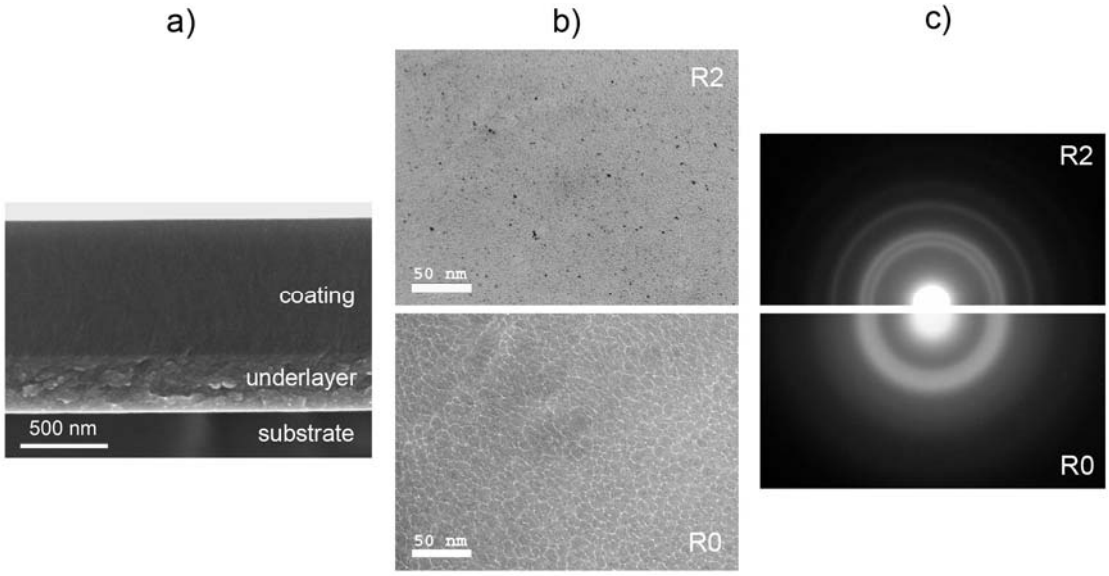
a)
b)
c)
coating
underlayer
500 nm
substrate
R2
50 nm
R0
50 nm
R2
R0

Figure 3

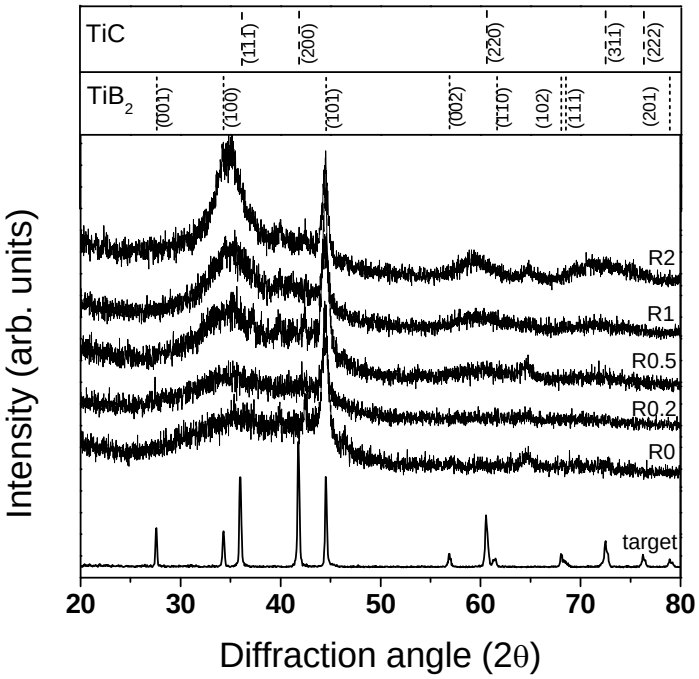
TiC
(111)
(200)
(220)
(311)
(222)
TiB2
(001)
(100)
(101)
(002)
(110)
(102)
(111)
(201)
R2
R1
R0.5
R0.2
R0
target
Intensity (arb. units)
20
30
40
50
60
70
80
Diffraction angle (2θ)

Figure 4

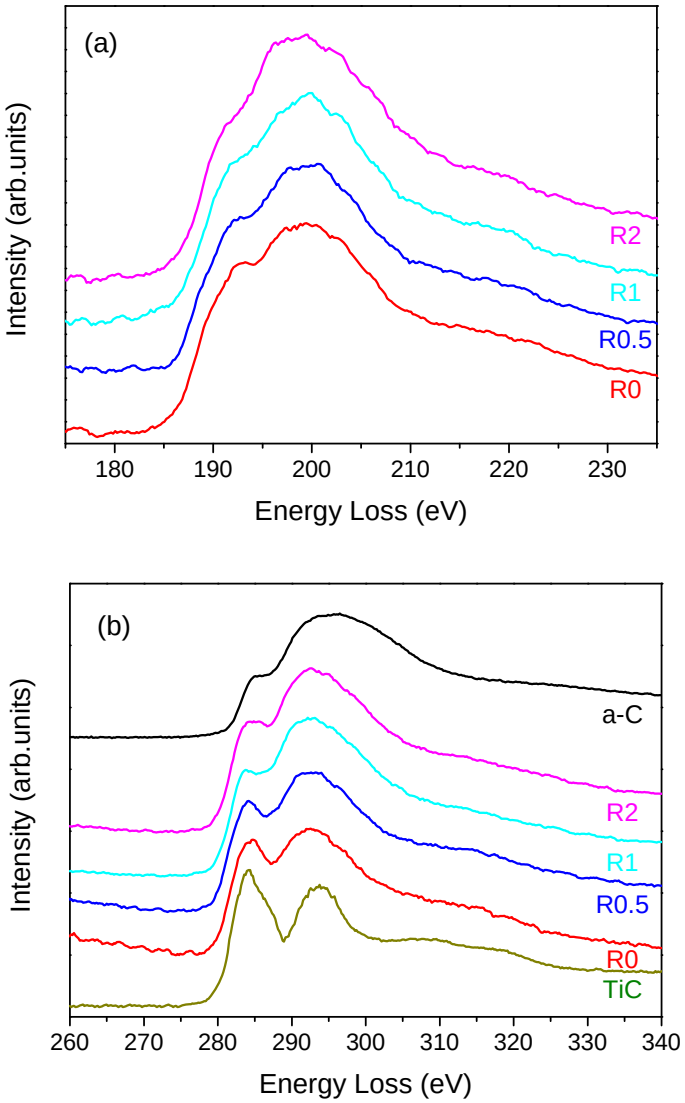
(a)
Intensity (arb.units)
R2
R1
R0.5
R0
180
190
200
210
220
230
Energy Loss (eV)
(b)
Intensity (arb.units)
a-C
R2
R1
R0.5
R0
TiC
260
270
280
290
300
310
320
330
340
Energy Loss (eV)

Figure 5

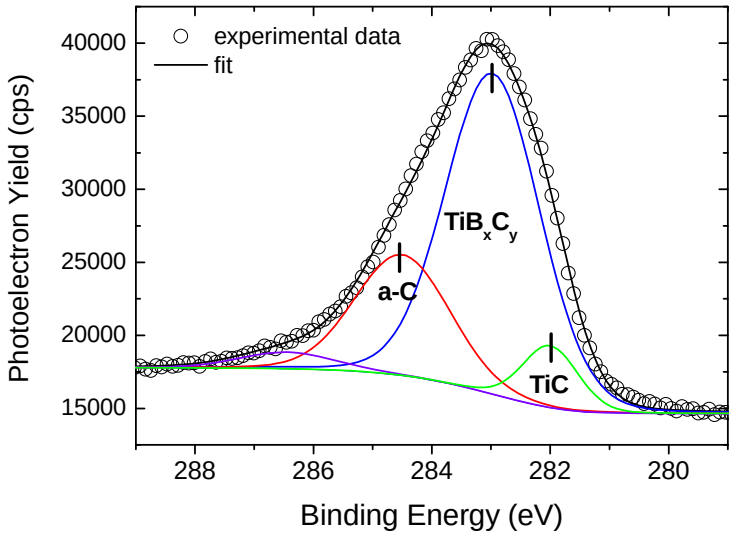
experimental data
fit
TiB$_x$C$_y$
a-C
TiC
Photoelectron Yield (cps)
Binding Energy (eV)
40000
35000
30000
25000
20000
15000
288
286
284
282
280